NASA CONTRACTOR REPORT

NASA CR-2528

NASA CR-2528

RAPID METHODS FOR CALCULATING RADIATION TRANSPORT IN THE ENTRY ENVIRONMENT

William E. Nicolet

Prepared by
AEROTHERM DIVISION/ACUREX CORPORATION
Mountain View, Calif. 94042
for Langley Research Center

NATIONAL AERONAUTICS AND SPACE ADMINISTRATION • WASHINGTON, D. C. • APRIL 1975

1. Report No.	2. Government Accession No.	3. Recipient's Catalog No.
NASA CR-2528		

4. Title and Subtitle	5. Report Date
RAPID METHODS FOR CALCULATING RADIATION TRANSPORT IN THE ENTRY ENVIRONMENT	April 1975
	6. Performing Organization Code
7. Author(s)	8. Performing Organization Report No.
William E. Nicolet	
	10. Work Unit No.
9. Performing Organization Name and Address	11. Contract or Grant No.
Aerotherm Division/ Acurex Corporation 485 Clyde Ave. Mountain View, CA 94042	NAS 1-12160
	13. Type of Report and Period Covered
12. Sponsoring Agency Name and Address	Contractor Report
National Aeronautics and Space Administration Washington, D. C. 20567	14. Sponsoring Agency Code

15. Supplementary Notes

FINAL REPORT

16. Abstract

A procedure is developed for the prediction of radiation transport events in the context of the entry heating environment. The equivalent-width and exponential approximations are employed to greatly reduce the computational requirements of the governing equations. Novel features are introduced in the use of an Elsasser band model to estimate line overlapping events and in the formulation of the wall reflection events. A matrix of calculations is presented to allow an assessment of the trade-offs between accuracy and computational efforts. It is concluded that the equivalent width model allows significant savings in computational effort with only modest penalties in accuracy. Consequently, the model should be viewed as an attractive candidate for use in radiation-coupled flow field prediction procedures.

17. Key Words (Suggested by Author(s))	18. Distribution Statement
High temperature gas radiation Entry environment Equivalent width approximation	Unclassified - Unlimited New Subject Category 34

19. Security Classif. (of this report)	20. Security Classif. (of this page)	21. No. of Pages	22. Price*
Unclassified	Unclassified	60	$4.25

*For sale by the National Technical Information Service, Springfield, Virginia 22151

FOREWORD

The present report describes extensions to and generalizations of a radiation transport calculation procedure developed over a period of several years at first the Aerotherm Corporation, then the Aerotherm Division of the Acurex Corporation, Mountain View, California. The initial effort was done under Contract NAS9-6719 for the NASA Manned Spacecraft Center, Structures and Mechanics Division. This effort included the development of the basic radiation properties and transport models. A subsequent effort was performed under Contract NAS1-9399 for Langley Research Center, Applied Material and Physics Division. On this effort, an equilibrium chemistry capability was incorporated into the procedure. The present effort was performed under Contract NAS1-12,160 for the Langley Research Center, Space Systems Division. On this effort the radiation transport procedure was generalized to allow the equivalent width approximation, molecular species properties associated with the Teflon and Silicon systems were added to the radiation model and the manner in which the far wings of the hydrogen lines are calculated was modified.

TABLE OF CONTENTS

LIST OF FIGURES

LIST OF TABLES

LIST OF SYMBOLS

B	Planck function
c	speed of light
d	frequency increment assigned to a line
E	black body emissive power for flux calculations, Planck function for intensity calculations
$\mathcal{E}_n$	exponential integral of order n
$F^{\pm}$	one sided radiative flux
$\Delta F^{\pm}$	one sided flux increment assigned to a line
f	oscillator strength of a line (f-number)
H, H_2, H_5 H_6, H_{10}	functions defined on page 71
h	Planck's constant
I_1, I_2	functions defined on page 19
J	wall radiosity
K	K=1 for intensity calculations, 2 for flux calculations
k	Boltzmann's constant
L	Ladenburg-Reiche function
m_e	mass of an electron
N	number density
n	principal quantum number

Q	partition function
q	net flux
r^w	wall reflectivity
S_h	effective homogeneous layer line strength
S	line strength
T_w	spectral flux assigned the line plus the continuum at the wall
X_h	homogeneous layer parameter defined by Equation 35
x	ionization potential
y_h	effective width of a homogeneous layer
y	spatial coordinate
$\bar{y}$	a particular spatial point
Z_1, Z_2	constants defined by Equations 20 and 21
W	line equivalent width

GREEK SYMBOLS

β_h	homogeneous layer parameter defined by Equation 36
γ_h	effective homogeneous layer (half) half width
η	density stretched wall normal coordinate
κ	mass absorption coefficient
γ	line half width
δ	path length

ε	emissivity
$\varepsilon_b^+, \varepsilon_b^-$	emissivity at wall (+) and at outer boundary (-)
μ	absorption coefficient
μ'	absorption coefficient corrected for induced emission
ν	photon frequency
τ	optical depth
ϕ	stretching parameter

SUBSCRIPTS

c	quantity evaluated at the center of a line
c	quantity associated with continuum radiation
h	property of a homogeneous layer
i	species i
j	absorbing level j
k	line k
ℓ	quantity associated with line radiation
w	quantity evaluated at the wall
δ	quantity evaluated at the outer edge
ν	spectral quantity

SUPERSCRIPTS

b	quantity evaluated at a spatial boundary

c	continuum quantity
L	line property
S	quantity due to the Stark effect
w	quantity evaluated at the wall

RAPID METHODS FOR CALCULATING RADIATION TRANSPORT IN THE ENTRY ENVIRONMENT

by

William E. Nicolet
Acurex Corporation

SECTION 1

INTRODUCTION

The ability to predict radiant energy transport is required in order to understand the heating phenomena associated with bodies entering planetary atmospheres at high velocities. The radiation transport is important both as an energy source in direct thermal contact and indirectly through the coupling between it at the thermal boundary layer. Quantitative predictions of radiative transport under these conditions require frequency dependent properties of the radiating species, a frequency dependent transport model and a method for predicting temperatures and species mole fractions, given the thermodynamic state conditions.

In a prior study (Reference 1), a procedure was developed for the prediction of the appropriate thermodynamic equilibrium and radiation transport events. This model has sufficient accuracy and requires modest computational efforts for applications where it is not coupled to a flow field procedure such as that of Sutton (Reference 2). For the coupled application, the radiation transport has to be evaluated at space stations (along the body) and at every (or a good fraction thereof) iteration. Such requirements can cause the total computational time to be measured in hours, even with modern computers. The purpose of the present study is to modify the existing (Reference 1) radiation transport model to significantly reduce the computing efforts while maintaining acceptable accuracy.

The radiation properties model is reviewed in Section 2; finite difference and equivalent width approaches for the line transport events are formulated in Section 3; a matrix of calculations is presented in Section 4; and concluding remarks are presented in Section 5. The calculations presented in Section 4 illustrate the advantage in computing effort obtained and the trade-offs against accuracy which are required.

SECTION 2

RADIATION PROPERTIES

The radiation properties model is based on that of Nicolet (Reference 1). Two essential approximations are retained, the bandless molecular band system and the line group approximation for the atomic lines. The present model differs from that of Reference 1 in the treatment of the half widths of some of the hydrogen lines, as will be discussed subsequently.

Molecular Band Model

The bands within each band system are smeared according to the scheme

$$\bar{\mu}_\nu = \int_{\Delta\nu} \mu_\nu d\nu/\Delta\nu$$

where the $\Delta\nu$ are selected such that the $\bar{\mu}_\nu$ varies smoothly. The "bandless model" obtained in this fashion is felt to be satisfactory for radiation heating calculations.

Atomic and Ionic Line Model

The line group approximation is employed to simplify the calculation. The frequency range of interest is divided into a number of frequency increments - 15 to 20 or thereabout. These are not necessarily connected. Each one defines as a line group those lines which are centered within it. The line contribution at a frequency point within a frequency increment is obtained by considering only those lines within its group. This approximation is valid unless all three of the following conditions are satisfied:

1. The path lengths are sufficiently long and the electron densities sufficiently high to lead to blanketing
2. The line group boundaries are placed in between closely spaced lines
3. The continuum intensities are not already black body

In addition, the line group approximation becomes inaccurate for extremely long path lengths where the equivalent width of an isolated line can become greater than the width of the line group. This occurs frequently in hydrogen rich atmospheres where the wings of each of the four stronger hydrogen lines (Lyman

alpha and beta and Balmer alpha and beta) can significantly exceed the boundaries of its line group. This problem is solved by assigning the far wing contributions to the continuum. The sketch illustrates the conditions where the line group approximation is valid (Figure 1a), introduces small errors (Figure 1b) and significant errors (Figure 1c).

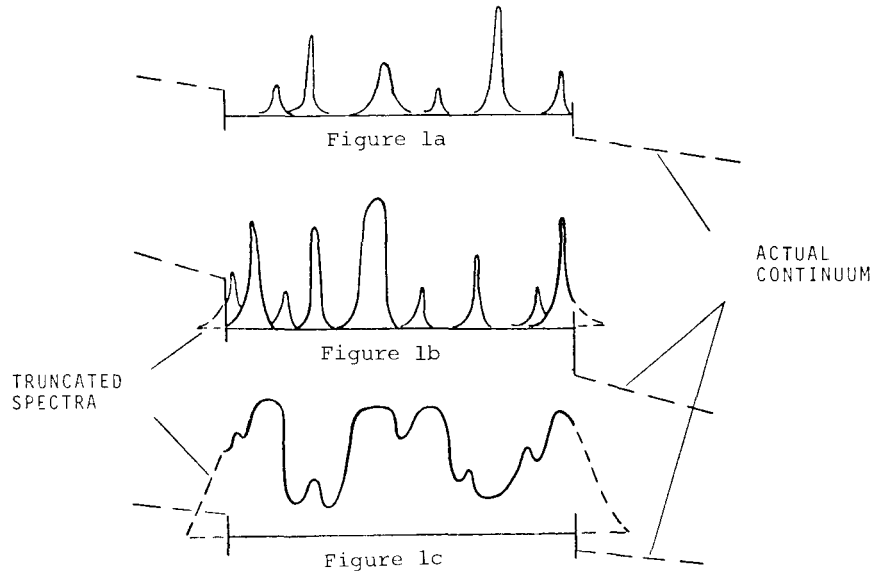

Figure 1. Intensities in the Line Group Approximation

Molecular Band Properties

The μ_ν values are from the calculations of Woodward (Reference 3), Biberman and Mnatsakanyan (Reference 4) and other reliable sources. Band systems are included for N_2 (1+,2+ and Birge-Hopfield), O_2 (Schumann-Runge), NO (γ, β, δ and ε), N_2^+ (1-), CN (Red and Violet), C_2 (Swan, Freymark and Mulliken), H_2 (Lyman and Werner) and CO (4+), all from the compilation of Nicolet (Reference 1). To this set, contributions have been added for the C_3 Swings band system, the SiO $A^1\Pi$-$X^1\Sigma^+$ band system and the CF $A^2\Sigma^+$-$X^2\Pi$ band systems.

The radiation properties model employs a C_3 Swings band cross section of 3×10^{-17} cm^2 which extends across the 3.0 to 3.5 ev region and which is temperature independent. This is consistent with the data of Brewer and Engelke (Reference 5) obtained in a furnace. Sufficient ficient information is not available to allow accurate extention of this data to high temperatures. The use of the low temperature cross sections

should be viewed as a method for obtaining estimates for the high temperature C_3 contribution.

The contribution of the CF $A^2\Sigma^+-X^2\Pi$ molecular band systems are from curve fits to radiation data generated with the Patch, Shackleford, and Penner "smeared line model" (Reference 6), employing an f-number (of .0167) and Franck-Condon factors obtained from Wentink and Isaacson (Reference 7). A sufficient set of molecular structure constants is available from the studies by Andrews and Barrow (Reference 8), Porter, Mann, and Acquista (Reference 9) and Thrush and Zwolenik (Reference 10).

The contributions of the SiO $A^1\Pi-X^1\Sigma^+$ molecular band system are also from curve fits to radiation properties generated with the smeared line model. The SiO f-number (of .13) is from the study of Smith and Liszt (Reference 11), while the Franck-Condon factors are from the study of Liszt and Smith (Reference 12).

Atomic Line Properties

With one exception, the hydrogenic lines considered individually employ line shapes from the studies of Griem (Reference 13) which consider electron and ion impact broadening. The exception is the half width relation for the high hydrogenic lines, derived originally as

$$\gamma_k^S = \text{const.} N_e \log_{10} \left(\frac{3 \times 10^6 T}{n_u^2 N_e} \frac{n_\ell^5 + n_u^5}{T^{1/2}} \right)$$

which was found to be inapplicable to many of the conditions encountered during entry into the large planets. The problem was found in Griem's use of a small argument expansion of an exponential integral during the original derivation. The elimination of the expansion yielded

$$\gamma_k^S = \text{const.} N_e \frac{(n_\ell^5 + n_u^5)}{T^{1/2}} \mathcal{E}_1^o(Y_{min})$$

where

$$\mathcal{E}_1^o(Y_{min}) = \int_{Y_{min}}^{\infty} \frac{e^{-Y}}{Y} dY$$

and

$$y_{min} = \frac{4\pi N_e}{3m_e}\left(\frac{e\,\hbar\,n_u^2}{kT}\right)$$

which are suitable for numerical evaluation.

Line properties are presented in Tables A.1, A.2, and A.3 in the appendix for a radiation model suitable for entry calculations for most of the atmospheres suggested for Jupiter, Saturn and Uranus, and a second radiation model which is suitable for Venus is presented in Table A.4. Some of the half-width data were obtained by estimate and are presented in parenthesis.

SECTION 3

TRANSPORT MODEL

Formulation

The basic equation governing the transfer of radiation through a medium in local thermodynamic equilibrium can be written as

$$\frac{dI_\nu}{dS} = \mu_\nu'(B_\nu - I_\nu) \tag{1}$$

where I_ν is the spectral intensity, B_ν is the Planck function, S is the ray length, μ_ν' is the absorption coefficient corrected for induced emission, viz.

$$\mu_\nu' = \mu_\nu[1 - \exp(-h\nu/kT)] \tag{2}$$

and μ_ν is the ordinary absorption coefficient.

In computing radiation fluxes across boundary and/or shock layers, it is convenient to make the tangent slab approximation. Thus, the properties along any ray can be related to those along the normal coordinate (y) by applying a cosine transformation, as shown in Figure 2. The resulting expressions for the optical depth, directional fluxes and total flux are well known and can be written in the form

$$\tilde{\tau}_\nu = \int_o^y \mu_\nu' dy \tag{3}$$

$$F_\nu^+(y) = \int_o^{\varepsilon_b^+} E_\nu(\varepsilon_\nu^+)\, d\varepsilon_\nu^+ \tag{4}$$

$$F_\nu^-(y) = \int_o^{\varepsilon_b^-} E_\nu(\varepsilon_\nu^-)\, d\varepsilon_\nu^- + 2J_\nu^w \mathcal{E}_3(\tau_\nu) \tag{5}$$

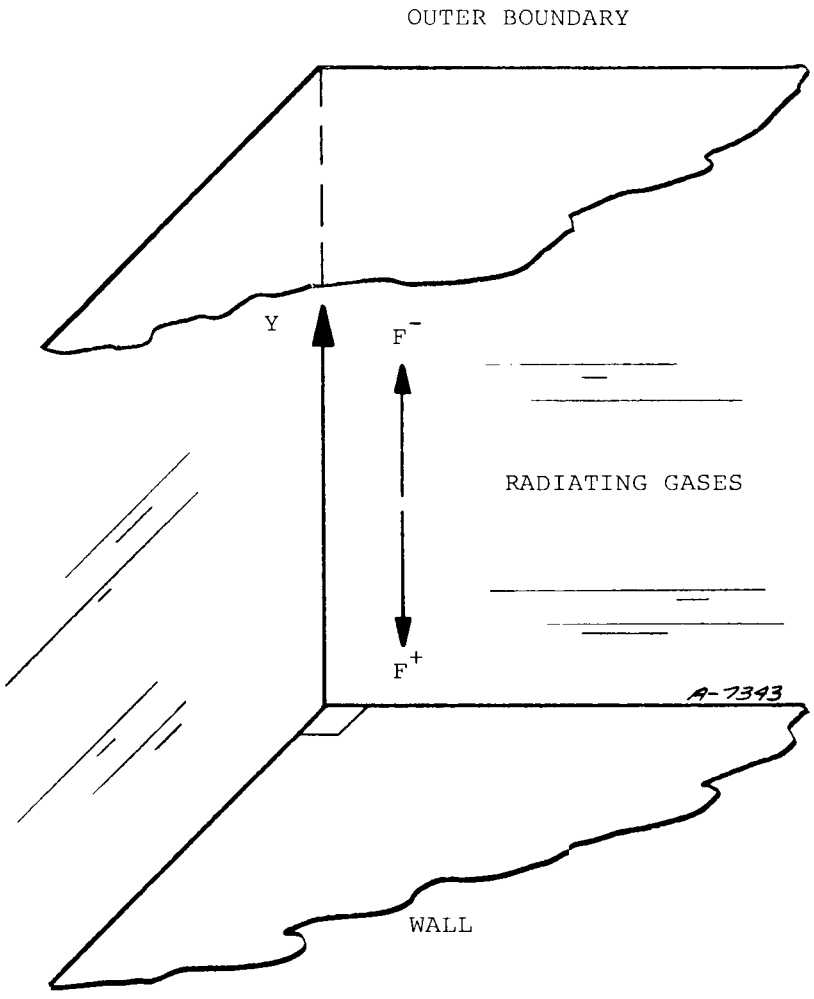

Figure 2. Radiating Layer Geometry

$$q_r(y) = \int_0^\infty [F_\nu^+(y) - F_\nu^-(y)]d\nu \tag{6}$$

where a diffuse wall has been assumed (reflectance r_ν^w and emittance ε_ν^w) and where E_ν and J_ν^w are the black body emissive power and wall radiosity, respectively, and are defined as

$$E_\nu = \pi B_\nu \tag{7}$$

$$J_\nu^w = \varepsilon_\nu^w E_\nu(0) + r_\nu^w F_\nu^+(0) \tag{8}$$

Finally, the emissivities ($\varepsilon_\nu^\pm$) are

$$\varepsilon_\nu^\pm = 1 - 2\mathscr{E}_3(|t_\nu - \tilde{\tau}_\nu|) \tag{9}$$

where the t_ν are dummy values of optical depth and the $\mathscr{E}_n(x)$ functions are exponential integrals of order n.

The exponential approximation can be used to further simplify the equations without an appreciable loss in accuracy for reentry problems. It is known (see Reference 14 for example) that when the approximation

$$2\mathscr{E}_3(x) \approx \exp(-2x) \tag{10}$$

is made, the transport solutions are exact in the optically thin limit, and of satisfactory accuracy in the optically thick limit. Thus, the emissitivites become

$$\varepsilon_\nu^\pm \approx 1 - \exp(-2|\tilde{\tau}_\nu - t_\nu|) \tag{11}$$

which are more convenient to work with than those given by Equation (5). Emissivities written in this form have the additional advantage that by surpressing the factor of 2 in the exponential arguments and replacing E by B in Equations (4) and (5), the same forumlation can be used to calculate intensities.

Additional simplification can be obtained for certain types of problems by employing a density stretched coordinate system. Introducing the transformation

$$\zeta d\eta = \rho\, dy \tag{12}$$

where

$$\zeta \neq \zeta(y)$$

yields

$$\tilde{\tau}_\nu = \zeta \int_0^\eta \kappa_\nu d\eta \tag{13}$$

for the optical depth. Here, the mass absorption coefficient

$$\kappa_\nu \equiv \mu'_\nu/\rho \tag{14}$$

has been introduced. A final transformation of the form

$$\tau \equiv 2\tilde{\tau}$$

introduces an optical depth variable which can be used directly as the exponential argument in Equation (11).

Before evaluating the transport integrals, it is advantageous to separate them into line and continuum parts. This offers several advantages in that (1) optimum coordinates can be selected in frequency space for the finite difference evaluation of the fluxes or (2) the transport integrals assume a form which is suitable for approximate evaluation by the equivalent width method and (3) an assessment of the importance of line effects is easily made from the results of each given set of calculations. Substituting μ_ν^C (or κ_ν^C) for μ_ν in Equations (2) to (5) yields corresponding values for $\tilde{\tau}_\nu^C$ and F_ν^C. where the $\pm$ signs have been dropped from the latter for brevity. The line contributions to the flux are obtained by difference

$$F_\nu^L \equiv F_\nu - F_\nu^C \tag{15}$$

where the F values are evaluated using the total absorption coefficient (line plus continuum). Thus, the line contribution is treated as a correction to the continuum flux.*

*It should be noted that the line contributions defined by Equation (15) can be negative for nonisothermal layers.

Finite Difference Evaluation of Line Fluxes

In the evaluation of the transport integrals, it is assumed that the logarithm of the integrands can be represented as linear functions of the independent variables between adjacent spatial nodes. Thus, the mass absorption coefficients become (suppressing ν subscripts for brevity)

$$\kappa(\eta) = \kappa_i \left(\frac{\kappa_{i+1}}{\kappa_i} \right)^{\frac{\eta - \eta_i}{\eta_{i+1} - \eta_i}} \tag{16}$$

and the black body emissive powers can be written as similar functions of the optical depths. Substituting the interpolation functions into Equations (3) to (14) and performing the integrations yields the increment in the exponential argument

$$\Delta\tau_{i,i+1} = 2\kappa_i \zeta (\eta_{i+1} - \eta_i) \frac{\left[\frac{\kappa_{i+1}}{\kappa_i} - 1 \right]}{\ell n \frac{\kappa_{i+1}}{\kappa_i}} \tag{17}$$

and recusion formulas for the directional fluxes

$$F_i^+ = e^{-\Delta\tau_{i,i+1}} \left\{ F_{i+1}^+ + \frac{E_i e^{\Delta\tau_{i,i+1}} - E_{i+1}}{1 + \frac{1}{\Delta\tau_{i,i+1}} \ell n \frac{E_i}{E_{i+1}}} \right\} \tag{18}$$

$$F_i^- = e^{-\Delta\tau_{i-1,i}} \left\{ F_{i-1}^- + \frac{E_i e^{\Delta\tau_{i-1,i}} - E_{i-1}}{1 + \frac{1}{\Delta\tau_{i-1,i}} \ell n \frac{E_i}{E_{i-1}}} \right\} \tag{19}$$

These equations are easily evaluated with two sweeps across the radiating layer provided that only one boundary is reflecting. The evaluation yields both directional fluxes at every node across the layer, consistent with the coupling requirements of most flow field procedures. Computationally, the use of the recursion formulas is much superior to a direct evaluation of Equations (4) and (5) and, under certain circumstances, comparable to the approximate equivalent

width approach, both of which require a sweep across the radiating layer for each pair of fluxes of interest. Moreover, the recursion formulas are suitably simple to be a point of departure for the development of influence coefficients (partial derivatives) required for some flow field coupling procedures. In view of these considerations, they were selected for numerical evaluation.

Equations (17) to (19) are to be evaluated at a number of frequency points selected to adequately describe the variation of the spectrum. In the case of atomic lines, the number is typically 1500 frequency points (100 lines with 15 points per line), which is large enough to cause the evaluation of the line integrals to dominate the computational effort.

To obtain the maximum accuracy for a given computational effort, a frequency grid must be selected for each line and should be dependent upon the characteristics of the layer as well as the individual line. This is accomplished by introducing a parameter ϕ which is characteristic of the width of the line (and will be discussed further in a subsequent paragraph) to stretch the coordinate system. The smallest increment and the distance to the most remote nodal point are defined by Equations (20) and (21), respectively, where $\tilde{\nu} = |\nu - \nu_c|$

$$\delta\tilde{\nu}_o = z_1\phi \tag{20}$$

$$\tilde{\nu}_{max} = z_2\phi \tag{21}$$

The quantities z_1 and z_2 are selected arbitrarily and are usually taken to be 0.5 and 10 (respectively), on this order. The intermediate nodal points are established using a growth law, viz.

$$\delta\tilde{\nu}_j = (1 + z)\delta\tilde{\nu}_{j-1} \tag{22}$$

where the nodal spacing increases (increasing subscript j) with increasing distance from the center of the line. The growth factor z is determined implicitly from the relation

$$\tilde{\nu}_{max} = \frac{(1 - z)^N - 1}{z}\,\delta\tilde{\nu}_o \tag{23}$$

where N is the number of increments to be used. Usually, the center of the line and about 5 to 7 additional points in each direction from it are sufficient.

The stretching parameter ϕ is defined by Equation (24).

$$\phi \equiv \gamma(\bar{y}) \sqrt{1 + \tau_c} \tag{24}$$

where the (half) half width $\gamma(\bar{y})$ is evaluated at a particular spatial location (usually as an edge condition) and τ_c is the optical depth of the entire layer at the frequency of the center of the line. It can be shown that ϕ has the following properties:

$$\lim_{\tau_c \to 0} \phi = \gamma(y) \tag{25}$$

$$\lim \phi \approx h\tilde{\nu}\Big|_{\tilde{\tau}_\nu = 1} \tag{26}$$

$$\gamma(\bar{y}) \Big/ \left[h\tilde{\nu}\Big|_{\tilde{\tau}_\nu = 1} \right] \to 0$$

That is, the ϕ is the distance in frequency space from the center of the line to the half intensity position when the line is weak, and it is approximately the distance to the frequency at which the layer has unit optical depth when the line is strong. At intermediate values of τ_c, ϕ should also be a reasonable approximation to the width of the line. Equations (20) to (26) specify the line frequency grid.

Equivalent Width Evaluation of Line Fluxes

Consider the absorption coefficient in a narrow spectral region $\delta\nu$ which contains an absorbing line. If $\delta\nu$ is sufficiently small, the continuum contribution to the absorption coefficient μ_c can be approximated as

$$\mu_c \neq f(\nu)$$

and the Planck function can be approximated as

$$E_\nu \neq f(\nu)$$

with little loss in accuracy. If $\delta\nu$ is also sufficiently wide to contain the line, the incremental contribution to the flux* directed toward the wall is, i.e.

*The remainder of this discussion will focus on the evaluation of the radiation flux, but is also applicable to the evaluation of the intensity.

$$\Delta F^{+}(0) = \int_{\delta\nu}\int_{o}^{\tilde{\tau}(\tilde{y})} Ee^{-\tilde{\tau}}\, dt\, d\nu \tag{27}$$

can be written as

$$\Delta F^{+}(0) = \Delta F_c^{+}(0) + \Delta F_\ell^{+}(0)$$

where the continuum component has its usual definition

$$\Delta F_c^{+}(0) = \delta\nu \int_{o}^{\tilde{\tau}_c} Ee^{-\tilde{\tau}_c}\, dt_c \tag{28}$$

$$\tilde{\tau}_c = K \int_{o}^{\tilde{y}} \mu_c dy \tag{29}$$

and where $\tilde{y}$ is the space coordinate measured from the point at which the flux is to be evaluated. The line component can be expressed as

$$\Delta F_\ell^{+}(0) = \int_{o}^{W(0)} Ed W^{+} \tag{30}$$

where the line equivalent width has been introduced

$$W^{+}(0) = e^{-\tilde{\tau}_c} \int_{\delta\nu} (1 - e^{-\tilde{\tau}_\ell})\, d\nu \tag{31}$$

where

$$\tilde{\tau}_\ell = K \int_{o}^{\tilde{y}} \mu_\ell dy. \tag{32}$$

but no additional approximations were imposed. The frequency integrations implicit in Equation (30) can be evaluated analytically for two interesting cases. Thus, Equation (30) reduces to

$$\Delta F_\ell^{+}\Big|_{\substack{\text{optically}\\ \text{thin}}} = \int_{o}^{\tilde{y}} Ed\left[\exp(-\tilde{\tau}_c) \int_{o}^{y'} S dy''\right] \tag{33}$$

for an isolated, optically thin line. Likewise, it reduces to

$$\Delta F_{\ell}^{+}\Big|_{\substack{\text{strong}\\ \text{line}}} = 2\int_{o}^{\tilde{y}} Ed\left[\exp(-\tilde{\tau}_{c})\sqrt{\int_{o}^{y'} S\gamma dy''}\right] \tag{34}$$

for an isolated strong line.*

In the Curtis-Godson approximation, the actual radiating layer is replaced by a homogenous layer which has approximately equivalent transport events. The homogenous layer is characterized by three parameters E_h, X_h and β_h, where E_h is the homogenous black body emissive power and the other two are defined as

$$X_h = \frac{S_h \gamma_h}{2\pi\gamma_h} \tag{35}$$

$$\beta_h = \frac{2\pi\gamma_h}{d} \tag{36}$$

where d is the mean line spacing and will be defined subsequently. It is reasonable to define the homogenous layer parameters by evaluating Equations (33) and (34) across a homogenous layer i.e.

$$y_h S_h E_h e^{-\tilde{\tau}_c} - \Delta F_{\ell}^{+}\Big|\text{optically thin} \tag{37}$$

and

$$2E_h e^{-\tilde{\tau}_c}\sqrt{S_h \gamma_h y_h} = \Delta F_{\ell}^{+}\Big|\text{strong line} \tag{38}$$

which yield

$$X_h = \frac{2}{\pi}\left(\frac{\Delta F_{\ell}^{+}|\text{optically thin}}{\Delta F_{\ell}^{+}|\text{strong line}}\right)^2 \tag{39}$$

*In this context, a strong line is defined as one in which the dominant radiative energy events occur in spectral regions far beyond the line half width, $|\nu-\nu_c| >> \gamma$.

$$\beta_h = \frac{\Delta F_\ell^+ | \text{optically thin}}{E_h X_h (e^{-\tilde{\tau}} c/d)} \tag{40}$$

the desired results in terms of properties of the non-homogenous layer which can be evaluated directly. The flux emanating from a homogenous layer then becomes

$$\Delta F_\ell^+ = E_h W_h^+ (X_h, \beta_h) \tag{41}$$

where $W_h^+(X_h, \beta_h)$ is the homogeneous equivalent width.

A variety of equations are available for predicting the equivalent width for a homogenous layer. Of these, possibly three are of interest to investigators studying radiation transport in the context of the entry environment. Thus, the equivalent width of an isolated line is given by the Ladenburg-Reiche formula

$$W^+ = d\beta_h L(X_h) \tag{42}$$

where $L(X_h)$ is the Ladenburg-Reiche function, which can be evaluated from well established exact or simple approximate analytic relations (References 15 and 16) or from tables. The equivalent width of an Elsasser band containing only strong lines is given by

$$W^+ = d \, \text{erf}\left(\beta_h \sqrt{\frac{X_h}{2}}\right) \tag{43}$$

while the equivalent width of a band containing only weak lines is

$$W^+ = d \, [1 - \exp(-\beta_h X_h)] \tag{44}$$

where a weak line is defined as being either optically thin or very strongly overlapped, after Plass (Reference 17). The regions of validity of these three complementary relations are presented in Figure 3, which is consistent with the recommendations of Plass (Reference 18).

Valid estimates to the radiation flux increments from a real system can be made using Equations (41) to (44) provided that certain conditions are met. Thus, Equations (42) and (43) are valid only where the lines have a Lorentz shape. In addition, Equation (43) is valid only when the real line overlapping

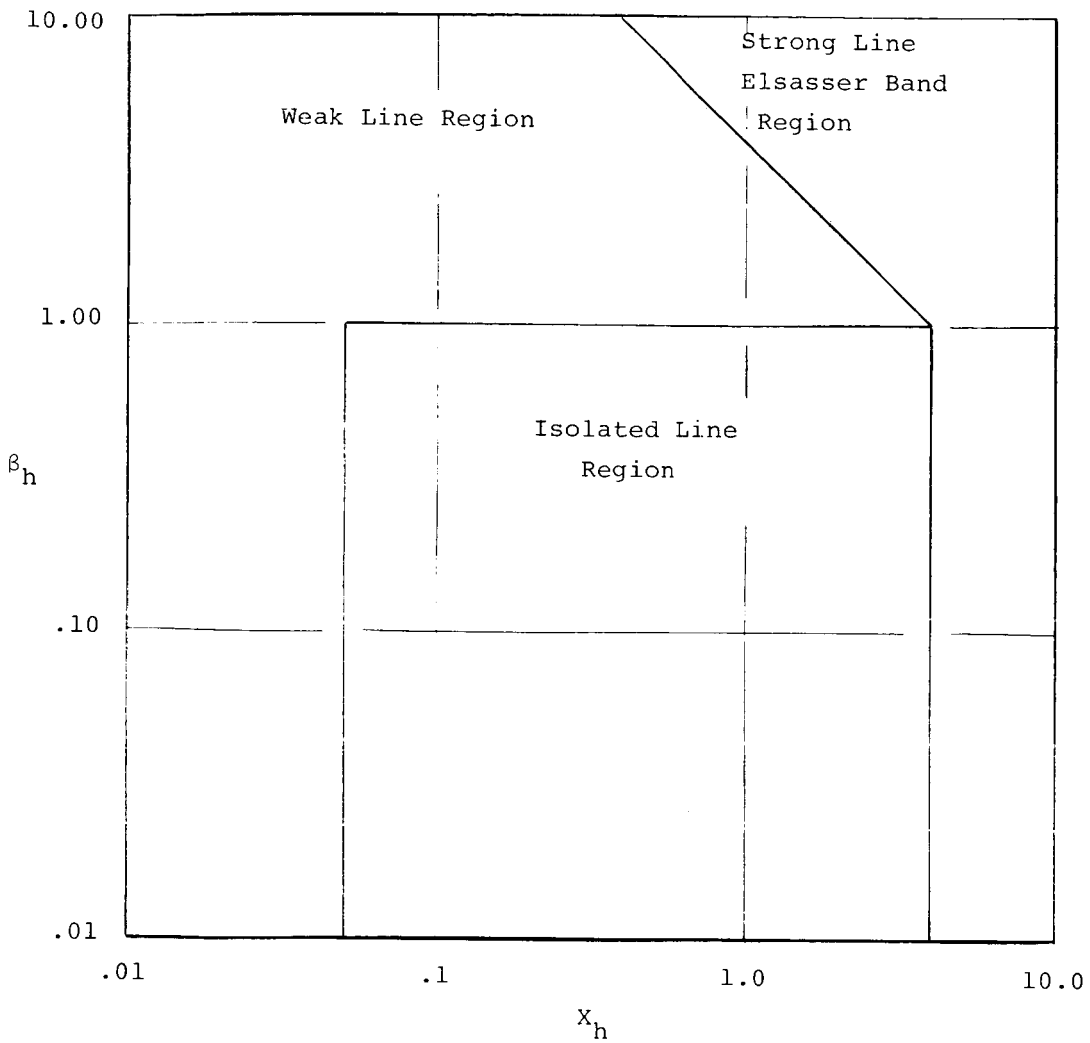

Figure 3. Regions of Validity for the Equivalent Width Formulas

events can be simulated through the use of the Elsasser model, a much more restrictive condition. However, it is felt that these conditions should be satisfied often enough for real systems to make the approach a useful one.

The evaluation of the governing relations (Equations (33), (34), (39), (40), (41) and (42), (43), or (44)) is straight-forward except for the evaluation of $\Delta F_\ell^+|_{\text{optically thin}}$ and $\Delta F_\ell^+|_{\text{strong line}}$. As written, each quantity requires two integrations across the layer for each node in space where the flux is to be evaluated. This effort can be reduced for $\Delta F_\ell^+|_{\text{optically thin}}$ by transforming Equation (33) to a coordinate system measured from the wall, y, $\tau_c(y)$, $t_c(y)$, i.e.

$$(\Delta F_\ell^+|_{\substack{\text{optically}\\ \text{thin}}})_i = e^{\tau_{c_i}}\left[\int_{y_i}^{y_e} Ed\left(e^{-t_c}\int_o^y Sdy\right) - \int_o^{y_i} Sdy \int_{y_i}^{y_e} Ede^{-t_c}\right] \tag{45}$$

which need be evaluated only once to yield the $\Delta F_\ell^+|_{\text{optically thin}}$ at all the spatial nodes across the layer. The integrations in Equations (34) and (45) are readily evaluated by assuming that the logarithm of each integrand is a linear function of its independent variable between adjacent spatial nodal points.

The governing relations for the radiative flux being transported away from the wall are similar to those presented here except for components due to wall reflection and emission which will be discussed subsequently.

Equivalent Width of Wall Emission and Reflection

The flux increment emanating from the wall includes components due to wall emission, continuum reflection and line reflection. Of these, the wall emission and continuum reflection components are treated in a straight-forward manner i.e.

$$\Delta F_{c_w}^- = d(r^w F_{c_w}^+ + \varepsilon^w E_w) \tag{46}$$

for a wall characterized by a reflectivity r^w, emissivity ε^w and black body emissive power E_w. The line reflection cannot be treated unambiguously under the existing assumptions, so it must be modeled.

Consider the flux increment incident upon the wall as being made up of a two step model (see Figure 4). The line component extends over a frequency increment W_w^+ where

$$W_w^+ \leq d$$

and has a spectral flux of $T_w - F_{c_w}^+$. The continuum component consists of the usual spectral flux F_c^+ and extends over the entire frequency range, d. With this boundary condition the optically thin flux increment becomes

$$\Delta F_\ell^- \Big|_{\text{thin}}^{\text{optically}} = \int_o^{\tilde{y}} Ed \left[\exp(-\tilde{\tau}_c) \int_o^{y'} S dy'' \right] \tag{47}$$

$$- F_c^- I_1$$

$$+ r^w (T_w - F_{c_w}^+) \left\{ W_w^+ - \min\left[W_w^+, I_1 \right] \right\}$$

where

$$I_1 = \exp(-\tau_c) \int_o^y S dy$$

Similarly, the strong line flux increment becomes

$$\Delta F_\ell^- \Big|_{\text{line}}^{\text{strong}} = 2 \int_o^{\tilde{y}} Ed \left[\exp(-\tilde{\tau}_c) \sqrt{\int_o^{y'} S\gamma dy''} \right] \tag{48}$$

$$- F_c^- I_2$$

$$+ r^w (T_w - F_{c_w}^+) \left\{ W_w^+ - \min\left[W_w^+, I_2 \right] \right\}$$

where

$$I_2 = 2\exp(-\tau_c) \sqrt{\int_o^y S\gamma dy'}$$

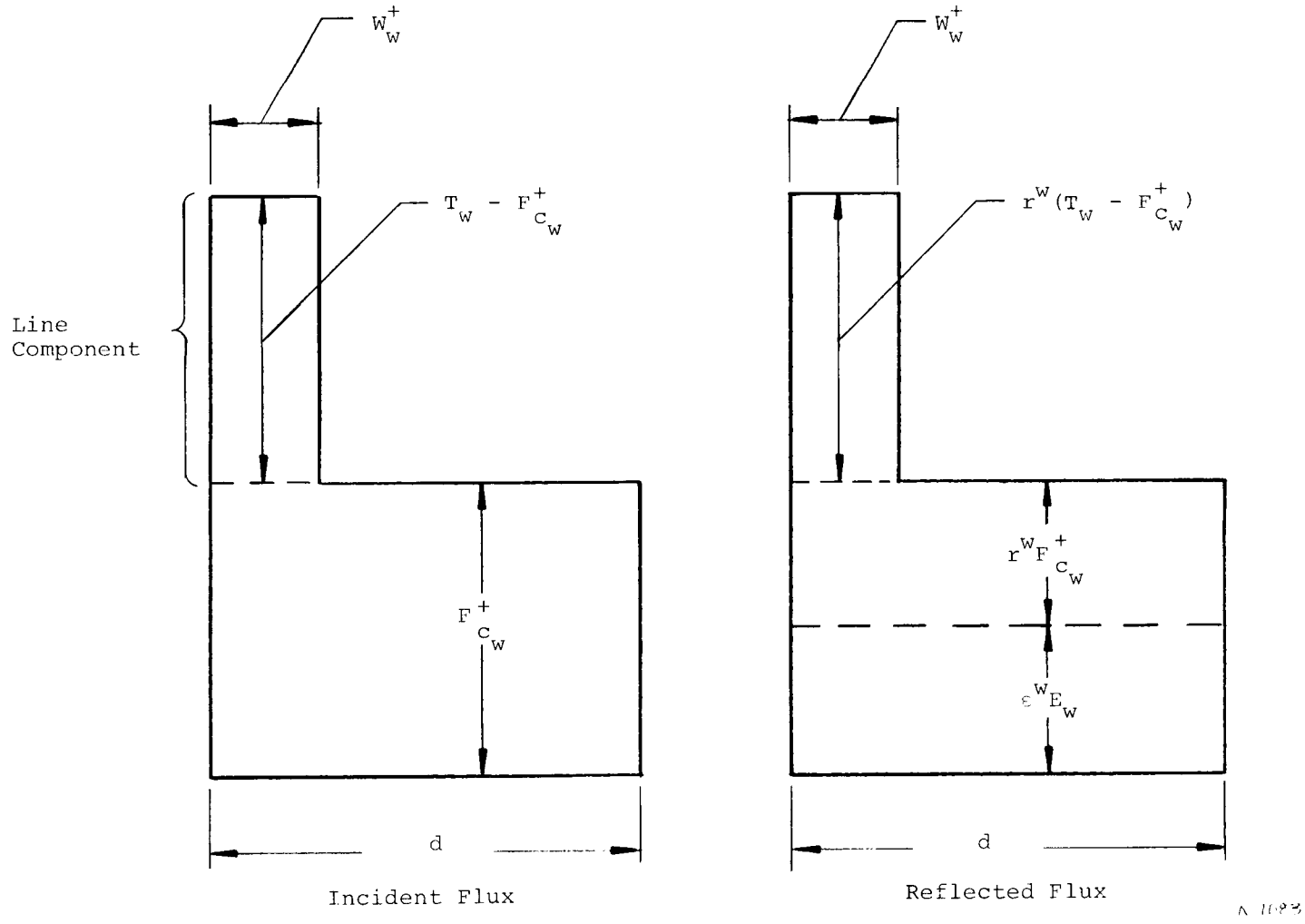

Figure 4. Flux Reflection Model

As before, the optically thin and strong line flux increments can be employed to define the homogeneous layer flux. Four relations are possible for differing ratios of W_w^+, I_1 and I_2.

Case 1: $I_2 < W_w^+$, $I_1 < W_w^+$

$$X_h = \frac{2}{\pi}\left[\frac{H}{H_{10}}\right]^2 \tag{49}$$

$$\beta_h = \frac{H}{H_2 X_h \exp(-\tau_c)} \tag{50}$$

Case 2: $I_2 < W_w^+$, $I_1 > W_w^+$

$$X_h = \frac{2}{\pi}\left[\frac{H_2 \Delta F_\ell^- \big| \text{optically thin}}{H_6 H_{10}}\right]^2 \tag{51}$$

$$\beta_h = \frac{\Delta F_\ell^- \big| \text{optically thin}}{H_6 X_h \exp(-\tau_c)} \tag{52}$$

Case 3: $I_2 > W_w^+$, $I_1 < W_w^+$

$$X_h = \frac{2}{\pi}\left[\frac{H\, H_6}{H_2 \Delta F_\ell^- \big| \text{strong line}}\right]^2 \tag{53}$$

$$\beta_h = \frac{H}{H_2 X_h \exp(-\tau_c)} \tag{54}$$

Case 4: $I_2 > W_w^+$, $I_1 > W_w^+$

$$X_h = \frac{2}{\pi}\left[\frac{\Delta F_\ell^- \big| \text{optically thin}}{\Delta F_\ell^- \big| \text{strong line}}\right]^2 \tag{55}$$

$$\beta_h = \left[\frac{\Delta F_\ell^- \big| \text{optically thin}}{H_2 X_h \exp(-\tau_c)}\right] \tag{56}$$

where the coefficients are defined by

$$H = \Delta F_{\ell}^{-}\Big|_{\text{thin}}^{\text{optically}} - H_5 \tag{57}$$

$$H_2 = E_h - r^w(T_w - F_{c_w}^{+}) - F_{c_w}^{-} \tag{58}$$

$$H_5 = r^w W_w^{+}(T_w - F_{c_w}^{+})\exp(-\tau_c) \tag{59}$$

$$H_6 = E_h - F_c^{-} \tag{60}$$

$$H_{10} = \Delta F_{\ell}^{-}\Big|_{\text{line}}^{\text{strong}} - H_5 \tag{61}$$

and are used in this form for all cases.

Equations (47) to (61) can be evaluated once the spectral flux incident upon the wall and the frequency increment W_w^{+} are evaluated. The usual equivalent width theory yields the product of these two quantities but not the quantities themselves, so new information must be introduced. This is not a difficult task for a truly homogeneous layer as a simple relation of the form

$$T_w - F_{c_w}^{+} \simeq (E_h - F_{c_w}^{+})\frac{X_h}{1 + X_h} \tag{70}$$

should be adequate. Note that Equation (70) is asymptotically correct for both large and small values of X_h. At intermediate values of X_h it should be of sufficient accuracy to meet the present requirements. Equation (70) was also selected for the general nonhomogeneous case. Its accuracy will depend on the effectiveness of the formulation in transforming a nonhomogeneous layer into a homogeneous one. Of course, the accuracy of the entire approach is strongly dependent upon this transformation, so that Equation (70) should not be viewed with any particular misgivings.

Having defined the line component of the spectral flux by Equation (70), the wall frequency increment is readily obtained from

$$W_w^{+} = \Delta F_{\ell_w}^{+} / (T_w - F_{c_w}^{+}) \tag{71}$$

which completes the two-step representation of the wall flux.

Selection of the Mean Line Spacing Parameter

In an Elsassor band, the mean line spacing parameter d represents the distance (in ev) between the centers of adjacent lines. This parameter plus the mean line strength determines how much growth the line can experience before its far wings begin to overlap and interact with the far wings of the other lines in the band. Of course, an Elsassor band with its equally spaced lines of equal strength is only roughly similar to the real spectra which exists in the high temperature plasmas of interest here. Thus, the selection of d must be made to make the overlapping of the far wings of the real spectra look as much like as possible those of the lines in an Elsassor band.

Consider the absorption coefficient at frequency ν_k due to the line centered at ν_i. Then

$$\mu_{i,k} = \frac{S_i \gamma_i}{\pi(\nu_k - \nu_i)^2} \tag{72}$$

where the strong line approximation $\nu_k - \nu_i >> \gamma_i$ has been invoked. At the same frequency, the contributions from all the other lines in the band is

$$\mu_k = \sum_{j \neq i} \frac{S_j \gamma_j}{\pi(\nu_j - \nu_j)^2} \tag{73}$$

If it is postulated that serious wing overlapping occurs when $\mu_k = \mu_{i,k}$, a significant frequency spacing parameter can be obtained from Equations (72) and (73) as

$$\nu_k - \nu_i = \sqrt{\frac{S_i \gamma_i}{\sum_{j \neq i} \frac{S_j \gamma_j}{(\nu_k - \nu_j)^2}}} \tag{74}$$

which was adopted as one-half the mean line spacing for the i^{th} line, i.e.,

$$d_i = 2 \sqrt{\frac{S_i \gamma_i}{\sum_{j \neq i} \frac{S_j \gamma_j}{(\nu_k - \nu_j)^2}}} \tag{75}$$

This relation is based on strong line approximations and will not be valid in the weak line or optically thin limits; of course, the details of line

overlapping events are not important in these limits, so this should not be an important limitation on its applicability.

The evaluation of d_i with Equation (75) is straightforward for radiating media which are uniform spatially. For nonuniform radiating media, either Equation (75) must be evaluated at conditions corresponding to those at a particular spatial point or some type of spatial averaging must be employed. In the present study, the first approach was adopted with the d_i being evaluated at $\bar{y}$.

The Radiation Transport Program (RAD/EQUIL/1973)

The entire solution procedure has been programmed for the UNIVAC 1108 and the CDC 6600 and 7600 machines. A description of the programs has been presented elsewhere (Reference 19). Typically, the equivalent width approach allows a factor of four increase in computing speed. The accuracy of the equivalent width approach vis-à-vis the finite difference approach will be discussed in Section 4.

SECTION 4

CALCULATIONS

A matrix of theoretical predictions has been obtained and is presented in this section. The object was to obtain a thorough understanding of the strengths and weaknesses of the equivalent width approximation as compared to the finite difference approximation. To this end, calculations were made comparing the fluxes of (1) an isolated line emanating from a homogeneous layer, (2) an isolated line plus a significant continuum emanating from a homogeneous layer, (3) an isolated hydrogen line plus a significant continuum emanating from a homogeneous layer, (4) an isolated line with a significant continuum and significant wall reflection, (5) a group of five identical lines in a line group emanating from a homogeneous layer, (6) a case including 20 line groups of varying features with the flux emanating from a nonhomogeneous layer, and (7) a general case with 20 line groups and a nonhomogeneous layer with varying elemental composition.

Isolated Line in a Homogeneous Layer

The predictions are presented in Table I for a radiating layer with optical properties of

$$E_\nu = 28{,}103 \quad \text{watts/(cm}^2 - \text{ev)}$$

$$\gamma = 0.0723 \quad \text{ev}$$

$$S = 8.42 \times 10^{-15} \quad \text{ev} - \text{cm}^{-1}$$

$$\mu_c = 0 \quad \text{cm}^{-1}$$

and where the width of the layer is treated as a parameter. For this problem, the equivalent-width approximation yields exact predictions. Thus, the ~ 5 percent comparison between the two sets of predictions should be viewed as a measure of the truncation errors inherent in the finite difference approximation. In the predictions to be presented subsequently, a 5 percent comparison should be viewed as a meaningful limit, with better comparisons being fortuitous.

TABLE I

HOMOGENEOUS LAYER

Layer Thickness δ (cm)	Line Flux Component at Wall (watts/cm^2)		Percent Difference
	Equivalent Width	Finite Difference	
.001684	.000057	.000059	3.4
.01684	.00018	.00018	-
.1684	.00060	.00058	3.3
1.684	.0019	.0018	5.3
16.84	.0060	.0059	1.67
168.4	.019	.019	-
336.9	.027	.026	3.7
842.2	.041	.040	2.4

Isolated Line Plus a Significant Continuum

The predictions are presented in Table II for a radiating layer with optical properties of

$$E_\upsilon = 31{,}326 \quad \text{watts/(cm}^2 - \text{ev)}$$

$$\gamma = 4.79 \times 10^{-5} \quad \text{ev}$$

$$S = 9.88 \times 10^{-3} \quad \text{ev} - \text{cm}^{-1}$$

$$\mu_c = 2.02 \times 10^{-3} \quad \text{cm}^{-1}$$

and where the width of the layer is treated as a parameter. Observe that the line contributions are linear at the shortest path lengths, reach a maximum at intermediate path lengths, then decrease to negligible values at the longest path lengths. Thus, the continuum and line radiation do not interact significantly at the shortest path lengths, whereas the continuum totally dominates the radiative events of the layer at the longest path lengths. The ~ 6 percent comparison indicates that the presence of a significant continuum should cause a slight degradation in the accuracy of the equivalent-width approximation. Overall, the comparison is viewed as satisfactory.

TABLE II

HOMOGENEOUS LAYER WITH A SIGNIFICANT CONTINUUM

Layer Thickness δ (cm)	Line Flux Component at Wall (watts/cm^2)		Percent Difference
	Equivalent Width	Finite Difference	
.00774	.088	.084	4.5
.0774	.82	.78	4.9
.774	4.8	4.7	2.
2.323	8.1	7.6	6.2
7.74	8.6	8.2	4.6
23.23	3.2	3.1	3.1
77.4	.026	.025	3.8
774.0	0.0	---	---

Isolated Hydrogen Line

The predictions are presented in Table III for a radiating layer with optical properties of

$$E_\nu = 28{,}103 \quad \text{watts/(cm}^2 - \text{ev)}$$

$$\gamma = 0.0723 \quad \text{ev}$$

$$S = 5.16 \quad \text{ev} - \text{cm}^{-1}$$

$$\mu_c = 2.31 \times 10^{-3} \quad \text{cm}^{-1}$$

and where the width of the layer is treated as a parameter. Hydrogen lines, with their large wing spans and distinctive shapes, should be viewed as poor candidates for treatment with the equivalent width approximation. Indeed, the ~ 41 percent comparison between the equivalent width and finite difference approximation for the line contributions is poor. Consequently, the equivalent width approximation is not generally recommended for hydrogen lines. It should be observed, however, that the two approximations are in fair agreement ~ 20 percent as long as the lines are important contributors to the total radiation (line plus continuum) of the line group. This point is illustrated by the numbers in parentheses in Table III which indicate fair accuracy ~ 14 percent for the calculation of the total radiation assigned to the line group. Thus, one might argue

that decent estimates to even hydrogen line contributions can be obtained using the equivalent width approximation.

TABLE III

HOMOGENEOUS LAYER WITH A HYDROGEN LINE AND A SIGNIFICANT CONTINUUM

Layer Thickness δ (cm)	Line Flux Component at Wall (watts/cm^2)		Percent Difference
	Equivalent Width	Finite Difference	
.864	130	120	7.6
8.64	1100	960	12.7
86.4	1700	1500	11.7
129.5	1100	920	16.3 (13.9)
172.7	700	540	23. (6.3)
259.1	230	170	26. (.5)
518.2	6	4	33. (.001)
863.6	.04	.02	41. ---

Isolated Line with a Reflecting Wall

The predictions are presented in Table IV for a radiating layer bounded on one side by a reflecting wall. The optical properties of the layer and wall are

$$E_\nu = 2{,}310 \quad \text{watts/(cm}^2 - \text{ev)}$$

$$\gamma = 2.58 \times 10^{-4} \quad \text{ev}$$

$$S = 17.86 \quad \text{ev} - \text{cm}^{-1}$$

$$\mu_c = 1.5 \times 10^{-2} \quad \text{cm}^{-1}$$

$$r^w = 0.6$$

$$\varepsilon^w = 0.4$$

and where the width of the layer is treated as a parameter. Predictions are given at varous spatial stations (across the layer) for the line flux component directed toward the bow shock (away from the wall). The ~ 10 percent comparison between the equivalent width and finite difference predictions represents some

TABLE IV

HOMOGENEOUS LAYER FLUX WITH

A REFLECTING WALL

Layer Thickness δ (cm)	Space Position y/δ	Line Flux Component Toward Shock (watts/cm^2)		Percent Difference
		Equivalent Width	Finite Difference	
.0126	0.0	.077	.073	5.2
	.25	.11	.10	9.1
	.50	.14	.13	7.1
	.75	.17	.16	5.9
	1.0	.20	.19	5.0
.03779	0.0	1.5	1.5	---
	.25	2.1	2.1	---
	.50	2.6	2.5	3.8
	.75	2.9	2.9	---
	1.0	3.2	3.2	---
.12596	0.0	3.1	3.0	3.2
	.25	4.2	4.2	---
	.50	4.9	5.0	2.0
	.75	5.3	5.6	5.4
	1.0	5.7	6.1	6.5
.37789	0.0	5.2	5.0	3.8
	.25	7.0	7.1	1.4
	.50	7.8	8.1	3.7
	.75	8.2	8.9	7.9
	1.0	8.5	9.4	9.6
3.7789	0.0	6.0	5.8	3.3
	.25	9.2	9.4	2.1
	.50	8.4	8.9	5.6
	.75	7.2	7.7	6.5
	1.0	6.0	6.5	7.7
37.789	0.0	.00084	.00084	---
	.25	1.2	1.2	---
	.50	.10	.10	---
	.75	.0079	.0078	1.2
	1.0	.00057	.00055	3.5

additional decay in the accuracy of the equivalent width approximation. However, the comparison is viewed as being satisfactory.

Homogeneous Layer with Five Identical Lines

The predictions are presented in Table V for a radiating layer with optical properties of

$$E_\nu = 1{,}646 \quad \text{watts/(cm}^2 - \text{ev)}$$

$$\gamma = 1.48 \times 10^{-5} \quad \text{ev}$$

$$S = 5.4 \times 10^{-4} \quad \text{ev} - \text{cm}^{-1}$$

$$\mu_c = 4.5 \times 10^{-8} \quad \text{cm}^{-1}$$

where the five identical lines are equally spaced across a frequency increment of 0.1 ev and where the width of the layer is treated as a parameter. The line group responds as five individual strong lines at the shorter path lengths, as an overlapped line system at the larger path lengths. The ~ 8 percent maximum difference occurs before overlapping effects become significant and can be assigned to inaccuracies which have been discussed previously. Thus, the effects of line overlapping do not appear to cause significant decay in the accuracy provided that the Elsasser model is a reasonable representation of the actual line group.

TABLE V

HOMOGENEOUS LAYER WITH FIVE IDENTICAL LINES

Layer Thickness δ (cm)	Line Flux Component at Wall (watts/cm^2)		Percent Difference
	Equivalent Width	Finite Difference	
.1	3.7	3.6	2.7
.3	6.4	6.2	3.1
1.0	12.0	11.0	8.3
3.0	20.0	19.0	5.0
10.0	33.0	32.0	3.0

TABLE VI

THERMODYNAMIC PROPERTIES DISTRIBUTION

Spatial Position	Temp (°K)	Pres. (atm)	Mole Fractions												
			O^+	O	N^+	N	C^+	C	O_2	CO	C_2	CN	C^-	O^-	E^-
0	8,663	1.201	9.7×10^{-4}	.634	4.2×10^{-5}	.0202	.0136	.291	5.4×10^{-5}	.024	1.1×10^{-4}	4.5×10^{-5}	2.6×10^{-6}	1.1×10^{-5}	.0147
.05	9,814	1.201	4.1×10^{-3}	.621	1.9×10^{-4}	.0192	.036	.275	2.3×10^{-5}	.0035	3.6×10^{-5}	1.2×10^{-5}	4.1×10^{-6}	1.8×10^{-5}	.040
.13	10,075	1.201	5.5×10^{-3}	.615	2.6×10^{-4}	.019	.043	.266	1.9×10^{-5}	.0023	2.7×10^{-5}	8.8×10^{-6}	4.4×10^{-6}	1.9×10^{-5}	.049
.25	10,291	1.200	6.9×10^{-3}	.609	3.3×10^{-4}	.0187	.049	.257	1.6×10^{-5}	.0017	2.2×10^{-5}	6.9×10^{-6}	4.5×10^{-6}	2.0×10^{-5}	.057
.38	10,407	1.199	7.8×10^{-3}	.605	3.8×10^{-4}	.0186	.053	.253	1.5×10^{-5}	.0014	2.0×10^{-5}	6.1×10^{-6}	4.6×10^{-6}	2.1×10^{-5}	.061
.50	10,486	1.196	8.4×10^{-3}	.602	4.1×10^{-4}	.0185	.056	.249	1.5×10^{-5}	.0013	1.8×10^{-5}	5.6×10^{-6}	4.7×10^{-6}	2.1×10^{-5}	.064
.63	10,544	1.192	8.9×10^{-3}	.600	4.4×10^{-4}	.0184	.057	.246	1.4×10^{-5}	.0011	1.7×10^{-5}	5.2×10^{-6}	4.7×10^{-6}	2.1×10^{-5}	.067
.75	10,590	1.185	9.4×10^{-3}	.598	4.6×10^{-4}	.0183	.059	.244	1.3×10^{-5}	.0011	1.6×10^{-5}	4.9×10^{-6}	4.7×10^{-6}	2.1×10^{-5}	.069
.88	10,633	1.177	9.8×10^{-3}	.597	4.8×10^{-4}	.0183	.061	.242	1.3×10^{-5}	9.9×10^{-4}	1.5×10^{-5}	4.7×10^{-6}	4.7×10^{-6}	2.1×10^{-5}	.071
1.00	10,690	1.164	1.0×10^{-2}	.594	5.1×10^{-4}	.0182	.063	.239	1.2×10^{-5}	9.0×10^{-4}	1.4×10^{-5}	4.3×10^{-6}	4.6×10^{-5}	2.1×10^{-5}	.0739

Nonhomogeneous Layer with Real Line Groups

The radiating layer is taken to have a width of 1.33 cm and thermodynamic properties as described in Table VI. There is assumed to exist a cold black wall bounding the layer on its low temperature side and a transparent shock wave boundary on the high temperature side. These are viewed as being typical of the inviscid flow region about a blunt probe in the Venus entry environment. The optical properties are modeled in terms of 20 line groups which are described in the appendix.

The important results are presented in Figures 5 and 6, where the fluxes toward the wall (Figure 5) and toward the shock wave (Figure 6) are presented as a function of spatial position for the total flux and a number of typical line groups. The comparisons are satisfactory, being within the 6 to 7 percent range for all the important line groups and for the totals. Moreover, the calculated flux at the wall is still more accurate, the comparison being within 2 to 3 percent. The equivalent width predictions tend to be consistently higher, so that one can assign some of the difference to truncation in the finite difference approximation. Indeed, one might view these predictions as upper and lower bounds on the real transport events.

The computing times for the UNIVAC 1108 are presented in Table VII.

TABLE VII

COMPUTING TIMES

Computation	Time (sec)	
	Finite Difference	Equivalent Width
Chemistry	3.994	3.994
Continuum Radiation	3.782	3.782
Line Radiation	82.343	7.082
Total	90.119	14.858

Thus, substantial savings in computational efforts can be obtained for a relatively small trade-off in accuracy. This should allow existing radiation-coupled procedures such as that of Sutton (Reference 1) to obtain comparable solutions for significantly reduced computational effort or, alternatively, allow consideration of additional physical events without significant additional computational penalty.

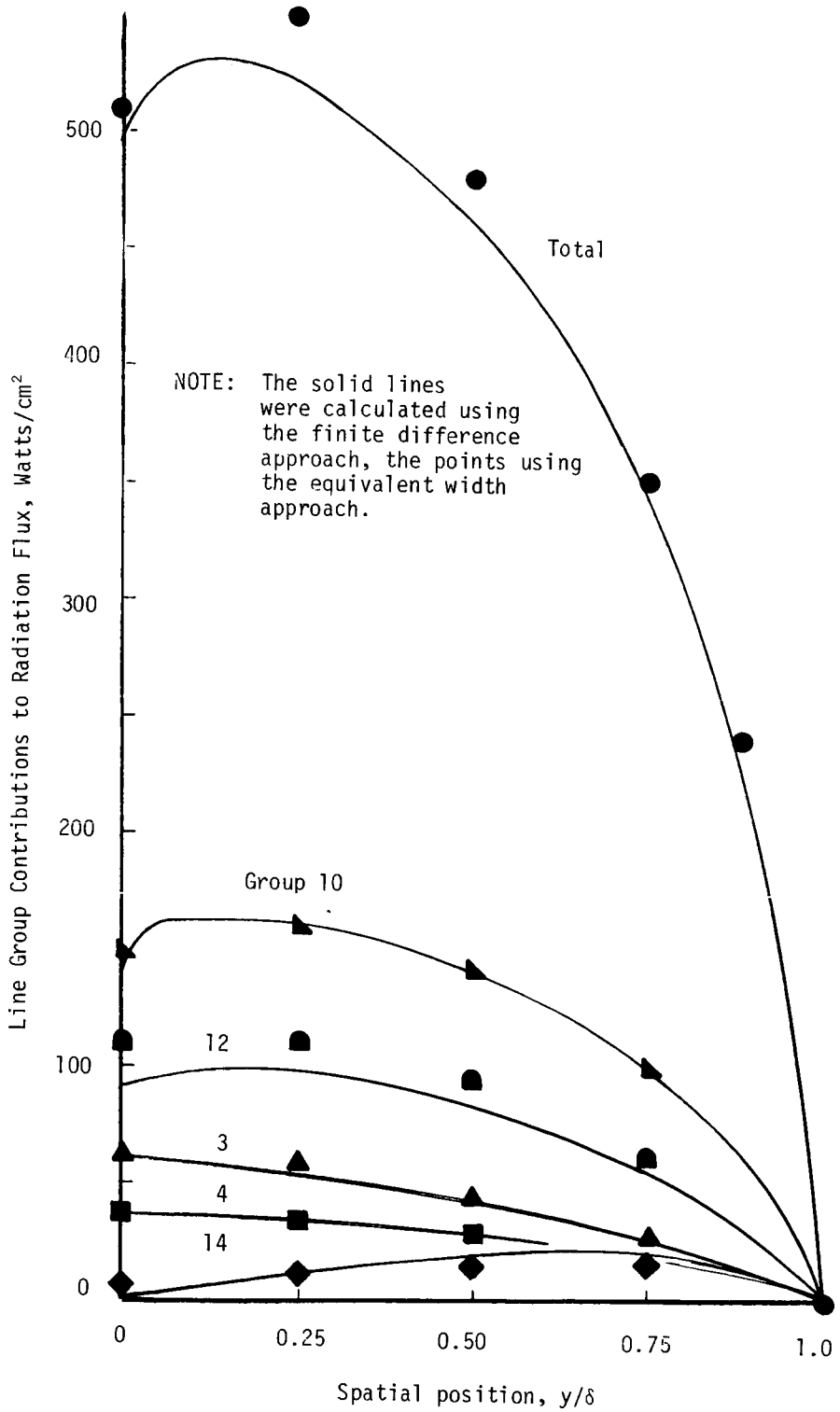

Figure 5. Flux Directed Toward Wall

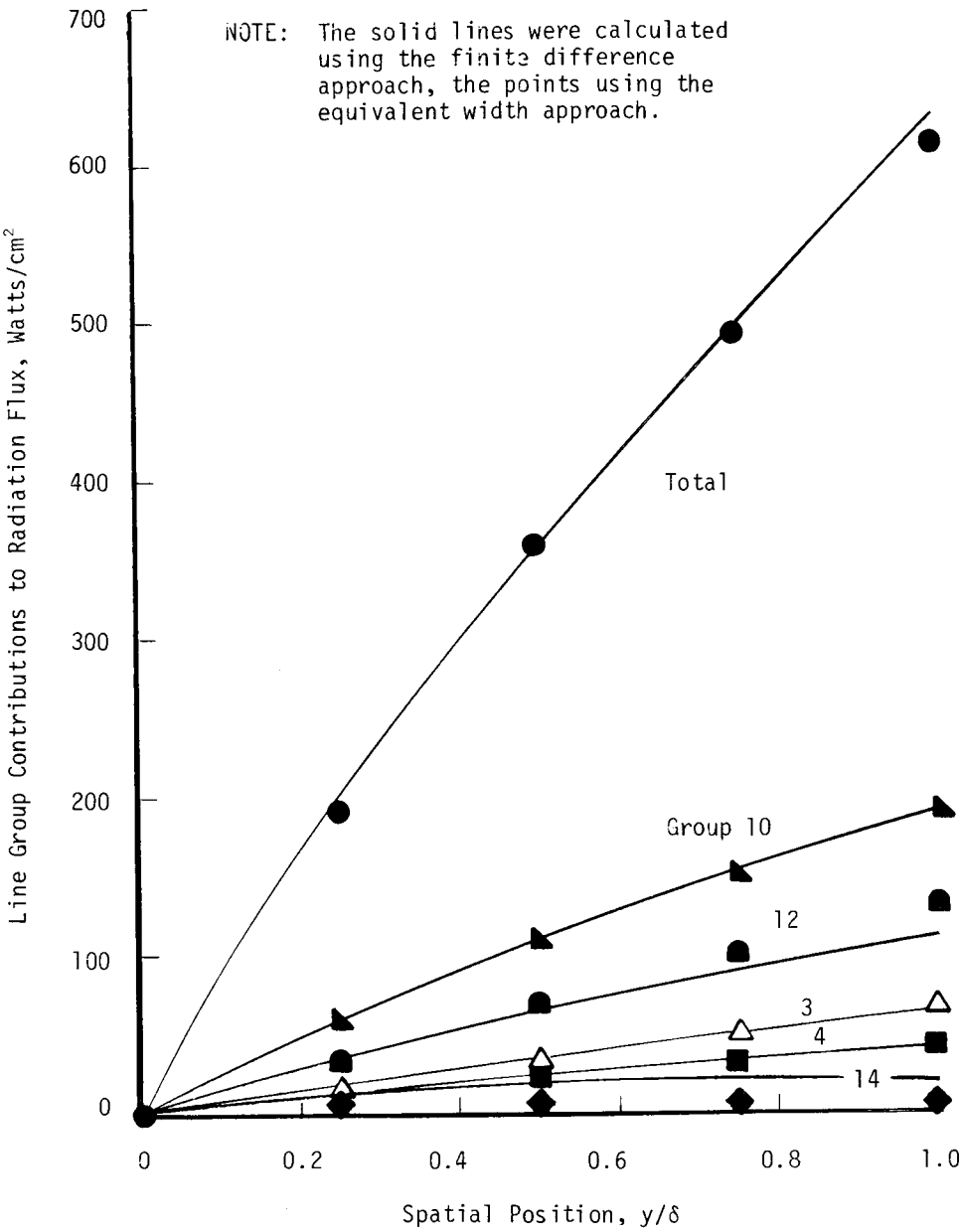

Figure 6. Flux Directed From Wall

Nonhomogeneous Layer with Varying Elemental Composition

The radiating layer is taken to have a width of 1.452 cm and thermodynamic properties obtained from a thermodynamic equilibrium calculation and the temperature, pressures and elemental compositions given in Table VIII. There is assumed to exist a cold black wall on its low temperature side and a transparent shock wave boundary on the high temperature side. These are viewed as being typical of the stagnation region shock layer about an ablating probe in the Venus entry environment. The optical properties are modeled in terms of 20 line groups, including hydrogen lines, which are described in Reference 19, under Sample Problem 5.

The important results are presented in Figures 7 and 8, where the fluxes toward the wall (Figure 7) and toward the shock wave (Figure 8) are presented as a function of spatial position for the total flux and a number of typical line groups. Most of the line groups show excellent comparisons, especially at the lower frequencies (lower group numbers). This suggests that the finite difference and equivalent width could be combined to good effect for certain types of problems. However, the line contributions to the flux differ by about 14 percent at the wall and about 15 percent in the interior, which is satisfactory for most flow field coupling problems. The continuum contributions to the flux values across the layer are comparable to the line contributions, so that the actual differences used in the flow field energy equation would be about one-half the values quoted above.

TABLE VIII

THERMODYNAMIC PROPERTY AND ELEMENTAL DISTRIBUTIONS*

Spatial		Temperature	Pressure	Elemental Mass Fractions			
Index	Position	(°K)	(atm)	X_H	X_C	X_N	X_O
1	0	3,772	3.43	3.495^{-2}	8.487^{-1}	4.005^{-3}	1.124^{-1}
2	0.0078	3,972		3.304^{-2}	8.433^{-1}	4.229^{-3}	1.194^{-1}
3	.0167	4,272		2.917^{-2}	8.228^{-1}	5.045^{-3}	1.430^{-1}
4	.0254	4,655		2.388^{-2}	7.668^{-1}	7.037^{-3}	2.023^{-1}
5	.0329	5,133		2.020^{-2}	6.702^{-1}	9.677^{-3}	2.999^{-1}
6	.0392	6,444		1.851^{-2}	5.915^{-1}	1.032^{-2}	3.796^{-1}
7	.0460	7,277		1.769^{-2}	5.345^{-1}	1.103^{-2}	4.368^{-1}
8	.0516	7,667		1.729^{-2}	4.908^{-1}	1.262^{-2}	4.793^{-1}
9	.0575	7,944		1.670^{-2}	4.457^{-1}	1.424^{-2}	5.234^{-1}
10	.0619	8,167		1.617^{-2}	4.166^{-1}	1.523^{-2}	5.520^{-1}
11	.0663	8,333		1.553^{-2}	3.902^{-1}	1.608^{-2}	5.782^{-1}
12	.0709	9,500	3.43	0	2.676^{-1}	1.930^{-2}	7.131^{-1}
13	.1641	10,763	3.42				
14	.2835	11,075	3.42				
15	.4029	11,270	3.41				
16	.5223	11,399	3.40				
17	.6418	11,501	3.39				
18	.7612	11,588	3.37				
19	1.0000	11,816	3.29				

*Superscripts indicate multiplication by that power of 10.

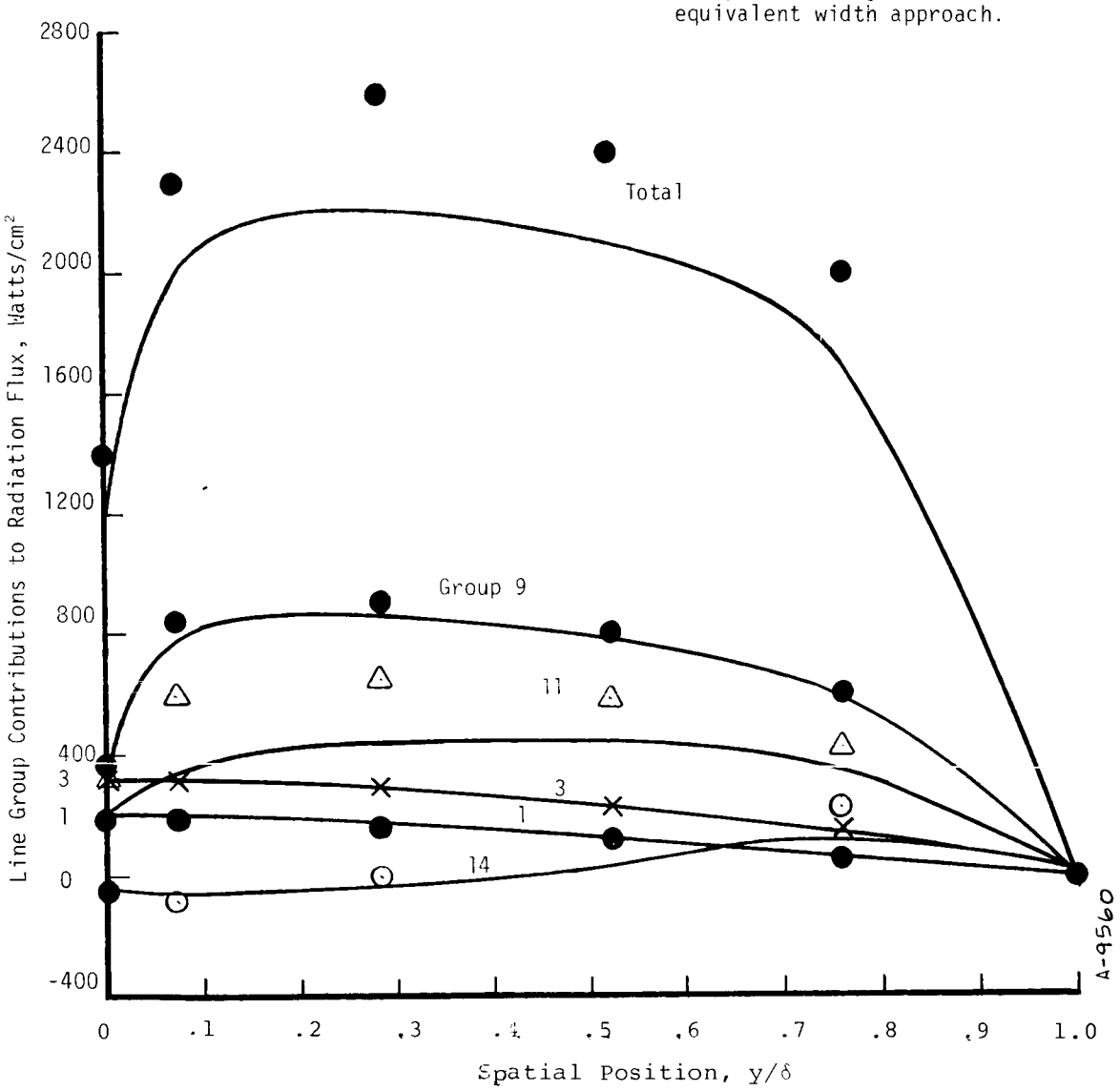

Figure 7. Flux directed toward wall with layer of varying elemental composition.

NOTE: The solid lines were calculated using the finite difference approach, the points using the equivalent width approach.

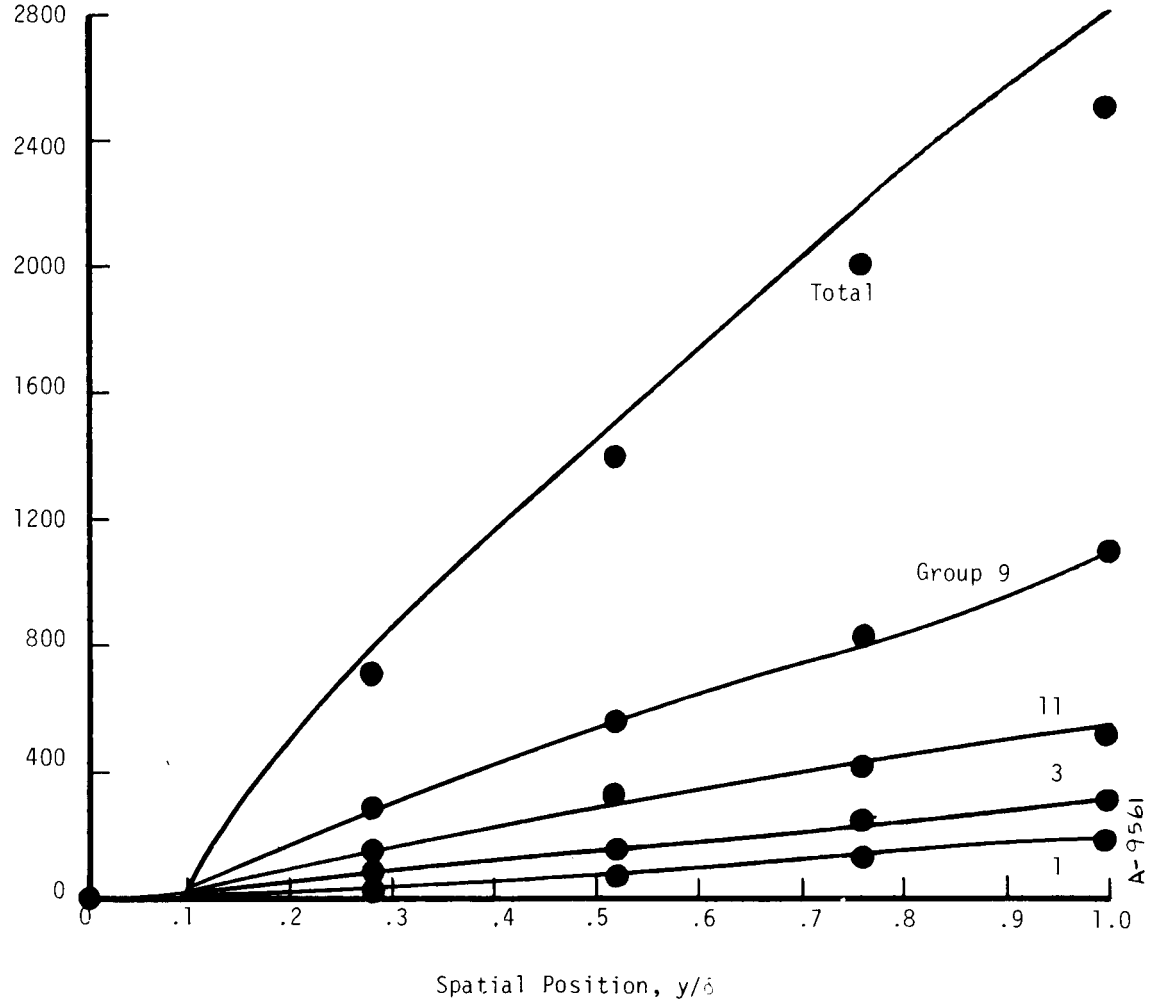

Figure 8. Flux directed from wall with layer of varying elemental composition.

SECTION 5

CONCLUDING REMARKS

A procedure has been developed for the evaluation of the line contributions for an interesting class of radiation transport problems. The following points might be made in summary:

- An equivalent width method has been formulated which considers continuum contributions and wall effects.
- A number of calculations have been performed to build confidence in the method.
- The comparisons with the finite difference procedure were all satisfactory with the possible exception of hydrogen lines.
- A savings of considerable computational effort should be possible for many radiation-coupled flow field procedures.

SECTION 6

REFERENCES

1. Nicolet, W. E.: Advanced Methods for Calculating Radiation Transport in Ablation-Product Contaminated Boundary Layers. NASA CR-1656, Aerotherm Corporation, Mountain View, California, September 1970.

2. Sutton, K.: Fully Coupled Nongray Radiating Gas Flows with Ablation Product Effects About Planetary Entry Bodies. AIAA Paper No. 73-672 presented at the Sixth Fluid and Plasma Dynamics Conference, Palm Springs, California, July 1973.

3. Woodward, H. T.: Predictions of Shock-Layer Radiation from Molecular Band Systems in Proposed Planetary Atmospheres. NASA Technical Note, NASA TN D-3850, Ames Research Center, Moffett Field, California, February 1967.

4. Biberman, L. M., Mnatsakanyan, A. Kh.: Optical Properties of Air in the Temperature Range from 4,000 to 10,000°K. Teplotizika Vysokikh Temperatur, 4, 148, 1966.

5. Brewer, L. and Engelke, J. L.: Spectrum of C_3. J. of Chem. Phys., Vol. 36, p. 992-998, 1962.

6. Patch, R. W., Schackleford, W. L., and Penner, S. S.: Approximate Spectral Absorption Coefficient Calculations for Electronic Band Systems Belonging to Diatomic Molecules. JQSRT, 2, 263, 1962.

7. Wentink, T. and Isaacson, L.: Oscillator Strengths of CF and Comments on Heats of Formation of CF and CF_2. J. of Chem. Phys., Vol. 46, No. 2, January 1967.

8. Andrews, E. B. and Barrow, R. F.: The Band-Spectrum of Carbon Monofluoride, CF. Proceeding of Physical Society of London, Vol. A64, p. 481, 1951.

9. Porter, T. L., Mann, D. E. and Acquista, N.: Emission Spectrum of CF. J. of Molecular Spectroscopy, Vol. 16, p. 228, 1965.

10. Thrush, B. A. and Zwolenik, J. J.: Predissociation in the Absorption Spectra of CF and CF_2. Transactions of the Faraday Society, Vol. 59, p. 582, 1963.

11. Smith, W. H. and Liszt, H. S.: Radiative Lifetimes and Absolute Oscillator Strengths for the SiO $A^1\Pi - X^1\Sigma^+$ Transition. J. Quantitative Spectroscopy and Radiative Transfer, Vol. 12, p. 505, 1972.

12. Liszt, H. S. and Smith, W. H.: RKR Franck-Condon Factors for Blue and Ultraviolet Transitions of Some Molecules of Astrophysical Interest and Some Comments on the Interstellar Abundance of CH, CH^+ and SiH^+. J. Quantitative Spectroscopy and Radiative Transfer, Vol. 12, p. 947, 1972.

13. Griem, H. T.: Stark Broadening of Higher Hydrogen and Hydrogen-Like Lines by Electrons and Ions. Astrophysical Journal, Vol. 132, p. 883, 1960.

14. Hunt, B. L. and Sibulkin M.: Radiation Transfer in a Gas of Uniform Properties in Local Thermodynamic Equilibrium. Part I, Part II, and Part III, Brown University. Report No. NONR-562(35)/18, 1966.

15. Kaplan, L. D. and Eggers, D. F.: Intensity and Line Width of the 15-Micron CO_2 Band, Determined by a Curve-of-Growth Method. J. of Chemical Physics, Vol. 25, No. 5, p. 876, November 1956.

16. Goldman, A.: Journal of Quantitative Spectroscopy and Radiative Transfer, Vol. 8, p. 829, 1968.

17. Plass, G. N.: Radiation from Nonisothermal Gases. Scientific Report No. 3, Southwest Center for Advanced Studies, Dallas, Texas, 18 June 1967. Also Air Force Cambridge Research Laboratories, Report No. AFCRL-67-0464, Office of Aerospace Research, United States Air Force, Bedford, Mass., 18 June 1967.

18. Plass, G. N.: Useful Representations for Measurements of Spectral Band Absorption. J. of Optical Society of America, Vol. 50, No. 9, p. 868, 1960.

19. Nicolet, W. E.: User's Manual for the 1973 Version of the Radiation Transfer Code (RAD/EQUIL Version 2). Acurex Report No. UM-73-10, Acurex Corporation, Mountain View, California, 1973.

APPENDIX A

TABULATED PROPERTIES

TABLE A.1

LINES AND LINE GROUPS FOR THE CHeH RADIATION MODEL

Specie	Center Frequency (ev)	Line Group Boundaries (ev)	Specie	Center Frequency (ev)	Line Group Boundaries (ev)
		← .1			
H	0.1662		C	1.487	
He	0.1667		He	1.7024	#6
He	0.2886	#1	He	1.7545	
H	0.3060				←1.79
H	0.4722				
		← .55	C	1.814	
			He	1.8562	#7
He	0.5869		H	1.888	
He	0.6022		He	2.1097	
He	0.6493				←2.4
H	0.660				
He	0.6629	#2	He	2.4714	
He	0.6633		He	2.5185	
C	0.6859		H	2.549	
C	0.710		He	2.7722	
He	0.7290		He	2.825	
		← .80	H	2.8559	#8
			He	2.9914	
He	0.8218		H	3.0221	
C	0.844	#3	He	3.0788	
C	0.852		He	3.0918	
		← .94	He	3.1266	
			He	3.1877	
He	0.9558		He	3.2453	
H	0.9671				←3.32
He	0.9691				
He	0.9695	#4	He	3.3457	
He	0.9894				←3.4 #9
C	1.019				
He	1.0356		He	3.4303	
C	1.0828		He	3.5955	#10
H	1.1333				←3.65
He	1.1445				
C	1.163				
		←1.2			
C	1.224	#5			
C	1.326				
		←1.4			

TABLE A.1 (Concluded)

Specie	Center Frequency (ev)	Line Group Boundaries (ev)
He	3.6952	
He	3.8886	#11
		←4.0
He	4.2090	
He	4.3816	#12
		←4.475
He	4.4851	#13
		←4.8
C	5.002	#14
		←6.2
C	6.424	
C	7.013	
C	7.078	
C	7.481	#15
C	7.717	
C	7.721	
C	7.947	
		←8.0
C	8.03	
C	8.191	
C	8.203	
C	8.302	
C	8.368	#16
C	8.377	
C	8.433	
C	8.474	
		←8.6

Specie	Center Frequency (ev)	Line Group Boundaries (ev)
		←9.0
C	9.137	
C	9.141	
C	9.332	
C	9.450	
C	9.611	
C	9.623	
C	9.697	#17
C	9.698	
C	9.709	
C	9.722	
C	9.797	
C	9.834	
C		
		←10.0
H	10.196	
C	10.401	
C	10.405	
C	10.714	
C	10.873	#18
C	10.875	
C	10.887	
C	10.986	
C	11.061	
		←11.2
		←11.2
H	12.084	#19
C	12.181	
		←12.2
H	12.745	
H	13.052	
C	13.119	#20
H	13.2182	
C	13.601	
		←13.8

TABLE A.2

DATA FOR HYDROGEN LINES

Transition Lower-Upper Quantum Numbers	Line Center		Statistical Weight of Lower Level	Oscillator Strength
	Wave Length (A)	Frequency (ev)	g_ℓ	f
LYMAN SERIES				
1-2 (L_α)	1,215.67	10.1968	2	0.4162
1-3 (L_β)	1,025.72	12.0852	2	0.07910
1-4 (L_γ)	972.54	12.7460	2	0.02899
1-5 (L_δ)	949.74	13.0520	2	0.01394
1-6 (L_ε)	937.80	13.2182	2	0.007799
BALMER SERIES				
2-3 (H_α)	6,562.8	1.8888	8	0.6407
2-4 (H_β)	4,861.32	2.5499	8	0.1193
2-5 (H_γ)	4,340.46	2.8559	8	0.04467
2-6 (H_δ)	4,101.73	3.0221	8	0.02209
PASCHEN SERIES				
3-4 (P_α)	18,751.	0.661	18	0.8421
3-5 (P_β)	12,818.	0.9671	18	0.1506
3-6 (P_γ)	10,938.	1.1333	18	0.05584
OTHERS				
4-5	40,512.	0.306	32	1.038
4-6	26,252.	0.4722	32	0.1793
5-6	74,578.	0.1662	50	1.231

TABLE A.3

DATA FOR HELIUM LINES*

Transition	Line Center Frequency (ev)	Half Width		Oscillator Strength f
		Per Free Electron at 10,000 K ($ev\text{-}cm^3$)	Temperature Exponent, n, in Eq. 1	
1s3s-1s3p (^1P)	0.1667	2.168^{-20}	-0.125	0.1572
1s3s-1s3p (^3P)	0.2886	1.041^{-20}	0.059	0.672
1s3p-1s4s (^3S)	0.5869	2.472^{-20}	0.292	0.1087
1s2s-1s2p (^1P)	0.6022	5.924^{-22}	0.386	0.3764
1s3p-1s4d (^1D)	0.6493	1.110^{-19}	-0.274	0.1617
1s3d-1s4f (^1F)	0.6629	(1.0^{-19})	(-0.2)	0.2525
1s3d-1s4f (^3F)	0.6633	(1.0^{-19})	(-0.2)	0.1042
1s3p-1s4d (^3D)	0.7290	(1.110^{-19})	(-0.274)	0.3615
1s3s-1s4p (^1P)	0.8218	9.541^{-20}	-0.138	0.035
1s3p-1s5d (^1D)	0.9558	(3.798^{-19})	-0.325	0.0347
1s3d-1s5f (^1F)	0.9691	(3.0^{-19})	(-0.2)	0.0395
1s3d-1s5f (^3F)	0.9695	(3.0^{-19})	(-0.2)	0.0346
1s3s-1s4p (^3P)	0.9894	4.415^{-20}	0.031	0.0321
1s3p-1s5d (^3D)	1.0356	(3.798^{-19}	(-0.2)	0.0922
1s2s-1s2p (^3P)	1.1445	3.297^{-22}	0.560	0.2695
1s2p-1s3s (^1S)	1.7024	(7.55^{-21})	0.331	0.0480
1s2p-1s3s (^3S)	1.7545	5.539^{-21}	0.331	0.0347
1s2p-1s3d (^1D)	1.8562	1.220^{-20}	-0.168	0.711
1s2p-1s3d (^3D)	2.1097	6.678^{-21}	0.025	0.609
1s2s-1s3p (^1P)	2.4714	2.168^{-20}	-0.125	0.1514
1s2p-1s4d (^1D)	2.5185	1.110^{-19}	-0.274	0.122
1s2p-1s4d (^3D)	2.7722	(1.110^{-19})	(-0.274)	0.125
1s2p-1s5d (^1D)	2.825	3.798^{-19}	-0.325	0.0436
1s2p-1s6d (^1D)	2.9914	(4.6^{-19})	(-0.1)	0.0213
1s2p-1s5d (^3D)	3.0788	(3.798^{-19})	(-0.2)	0.0474
1s2p-1s7d (^1D)	3.0918	(7.9^{-20})	(-0.2)	0.0112
1s2s-1s4p (^1P)	3.1266	9.541^{-20}	-0.138	0.0507
1s2s-1s3p (^3P)	3.1877	1.041^{-20}	0.059	0.09478
1s2p-1s6d (^3D)	3.2453	(4.6^{-19})	(-0.2)	0.0215
1s2p-1s7d (^3D)	3.3457	(7.9^{-19})	(-0.2)	0.0152
1s2s-1s5p (^1P)	3.4303	2.506^{-19}	-0.160	0.0221
1s2s-1s6p (^1P)	3.5955	5.765^{-19}	-0.173	0.0128
1s2s-1s7p (^1P)	3.6952	1.145^{-18}	-0.173	0.0066
1s2s-1s4p (^3P)	3.8886	4.415^{-20}	0.031	0.0505
1s2s-1s5p (^3P)	4.2090	1.375^{-19}	0.005	0.0293
1s2s-1s6p (^3P)	4.3816	3.253^{-19}	-0.021	0.0169
1s2s-1s7p (^3P)	4.4851	(7.9^{-19})	(-0.2)	0.0111

*Numerical superscrips indicate multiplication by that power of 10

TABLE A.4

LINES AND LINE GROUPS FOR THE CON RADIATION MODEL

Specie	Center Frequency (ev)	Line Group Boundaries (ev)
		← .6
O	.685	
C	.686	
N	.689	#1
C	.710	
N	.752	
		← .8
		← .81
C	.844	
C	.852	
N	.875	#2
O	.884	
N	.916	
N	.930	
		← .95
		← .96
N	.965	
O	.991	
C	1.019	
N	1.036	#3
C	1.083	
O	1.098	
O	1.132	
C	1.163	
		←1.2
C	1.224	
N	1.261	
N	1.319	#4
C	1.326	
O	1.338	
N	1.368	
		←1.4
N	1.438	
O	1.467	
C	1.487	#5
N	1.553	
O	1.594	
		←1.6

Specie	Center Frequency (ev)	Line Group Boundaries (ev)
		←1.62
N	1.663	
O	1.767	
C	1.814	#6
N	1.836	
O	2.015	
		←2.4
N	2.925	
O	3.000	#7
O	3.167	
N	3.472	
		←3.5
		←3.4
O	3.711	#8
		←4.0
C	5.002	#9
		←6.0
		←6.2
C	6.424	
C	7.013	
C	7.078	
N	7.111	#10
C	7.481	
C	7.717	
C	7.721	
C	7.947	
		←8.0
C	8.030	
C	8.191	
C	8.203	
C	8.302	
N	8.302	#11
C	8.368	
C	8.377	
C	8.433	
C	8.474	
N	8.781	
		←9.0

TABLE A.4 (Continued)

Specie	Center Frequency (ev)	Line Group Boundaries (ev)
		← 8.8
C	9.139	
N	9.301	
C	9.332	
N	9.394	
C	9.450	#12
N	9.460	
O	9.501	
C	9.612	
C	9.697	
		←10.
		← 9.7
C	9.709	
C	9.722	
C	9.797	
C	9.834	
N	9.973	
N	10.102	#13
O	10.182	
N	10.332	
C	10.401	
C	10.405	
N	10.418	
		←10.45
N	10.493	
N	10.585	
N	10.619	
N	10.682	
C	10.714	
N	10.757	
O	10.761	
		←10.8
C	10.873	
C	10.875	
C	10.887	#15
N	10.927	

Specie	Center Frequency (ev)	Line Group Boundaries (ev)
C	10.986	#15
O	11.007	
C	11.061	
N	11.200	
N	11.293	
N	11.310	
N	11.424	
N	11.609	
		←11.7
N	11.776	
O	11.806	
O	11.852	
N	11.874	#16
N	11.948	
N	12.000	
O	12.067	
		←12.1
O	12.160	
C	12.181	
N	12.316	
O	12.404	#17
N	12.414	
N	12.511	
O	12.521	
O	12.651	
		←12.8
N	12.877	
N	13.004	#18
C	13.119	
N	13.190	
		←13.4
N	13.508	
N	13.543	#19
C	13.601	
N	13.677	
		←13.8

TABLE A.4 (Concluded)

Specie	Center Frequency (ev)	Line Group Boundaries (ev)
N	13.993	←13.8
N	14.160	#20
N	14.257	
N	14.332	←14.5